Analytical Methods

COMMUNICATION

View Article Online
View Journal | View Issue

Cite this: *Anal. Methods*, 2015, 7, 3676

Received 19th January 2015
Accepted 28th March 2015

DOI: 10.1039/c5ay00148j

www.rsc.org/methods

An electrospun micro/nanofibrous mesh based nontoxic sensor for optical detection of high humidity†

Tianyu Wang, Hongxia Fu, Xinrui Duan* and Zhengping Li*

Optical transition of a polyethylene oxide electrospun micro/nanofibrous mesh from opaque to transparent has been studied by UV-Vis spectroscopy and scanning electron microscopy. This transition occurs only above approximately 88% relative humidity and could be used for humidity monitoring by the naked eye for food quality control in which low toxicity and irreversibility are highly required.

Humidity sensors are in great demand for many applications, such as food and pharmaceutical quality monitoring, air conditioning systems, and medical equipment.[1] Lots of effort has been made to develop humidity sensors with different sensing mechanisms, such as electrical[2] and optical[3] detection. Humidity has a great impact on the germination of microorganisms in food.[4] Especially when humidity is higher than approximately 85–90%, moulds and yeasts that frequently infest cereals and rice are significantly increased.[5] An effective humidity sensor for foods should be able to mark whether they have been exposed to critical humidity levels during their storage or not, regardless of the current humidity levels, namely, an irreversible humidity sensor. A safe, equipment-free, irreversible, and cheap sensor that could possibly be placed on each package of rice or cereals will help us to identify the risk before use.

Compared with electrical measurement based methods, colorimetric detection based sensors are usually cheap and do not require equipment. The color change of cobalt(II) chloride salt under different humidity conditions has been used as a test paper format in semiconductor packaging and desiccant monitoring due to its low cost. Mutagenic and carcinogenic cobalt chloride has been reported.[6a] Due to its relatively low toxicity, copper chloride salt has been used to manufacture cobalt-free humidity indicator cards. Direct contact with copper chloride still can cause acute toxicity, skin irritation, and serious eye damage. Thus these metal chloride salt based sensors are not ideal when low toxicity is required.[6b,c] Photonic crystal sensors have highly sensitive optical response to changes in humidity; unfortunately, most of them are still reversible sensors.[7]

Electrospinning is a simple and efficient tool to fabricate micro/nanofibrous membranes, and it has been widely used in tissue engineering and gas molecule sensing.[8] The large surface area of the electrospun fibrous mesh makes it a good platform for gaseous analyte detection.[9] Usually, a "sensing element" needs to be doped into fibers or modified onto fiber surfaces to achieve detection.[10] As far as we know, the optical properties of electrospun micro/nanofibers for detection purposes have not been explored yet.

It is well known that homogenous thin films of many polymers, for example polystyrene, poly(methyl methacrylate), and polyethylene oxide (PEO), are almost transparent to visible light and their corresponding electrospun fibrous mesh is opaque due to light scattering at the greatly increased air/fiber interface. In the vapor of an appropriate solvent, fibers should gradually fuse to each other and eventually form a homogenous thin film, and the opaque fibrous mesh will become transparent. Apparently, it will be an irreversible process.

In this work, we chose a water soluble and nontoxic polymer polyethylene oxide (PEO) to develop a safe and irreversible humidity sensor based on the above mechanism. PEO is well-known as a low toxic polymer and has been used in pharmaceuticals, skin creams, and toothpastes, even used as food additives.[11] The resulting opaque electrospun fiber mesh became transparent in 10 min under a high relative humidity environment. Later we used scanning electron microscopy imaging to investigate the change of morphology of the fibrous mesh during transition. Responses of the PEO electrospun fibrous mesh under different relative humidity conditions were studied as well.

Electrospinning technology is a versatile and effective method to fabricate fibers of several tens to hundreds of

Key Laboratory of Analytical Chemistry for Life Science of Shaanxi Province, School of Chemistry and Chemical Engineering, Shaanxi Normal University, Xi'an, Shaanxi, 710119, P. R. China. E-mail: duanxr@snnu.edu.cn; lzpbd@snnu.edu.cn

† Electronic supplementary information (ESI) available. See DOI: 10.1039/c5ay00148j

nanometers diameter from various materials, and PEO is one of the most frequently used materials to produce electrospun fibers.[8] Electrospinning was performed on a home-made electrospinning setup. Our PEO fibrous mesh was produced by electrospinning 1 mL of 4% w/v PEO solution for 1 hour in a humidity controlled cubic chamber at room temperature. A piece of grounded aluminium foil was used as a stationary grounded collector. The distance from the tip to the needle is 12 cm and the voltage was set at 4 kV during electrospinning. Humidity was monitored with a digital humidity and temperature thermometer during electrospinning and controlled by a N_2 gas flow. From the scanning electron microscopy (SEM) image shown in Fig. 1a, we can clearly see a fibrous structure. The diameter of electrospun fibers is 0.94 ± 0.20 μm. The PEO polymer solution was transparent (Fig. 1b, inset image). After electrospinning, since light scattering occurs at the interface of air/fiber and due to the random orientation of fibers, incident light will be blocked; thus the electrospun fibrous mesh appears to be opaque and white in color (Fig. 1b).

After the electrospinning process, the resulting fibrous mesh was transferred from the aluminium foil onto an optical clear adhesive film that is usually for 96 well plate sealing, which has much higher mechanical strength than an electrospun fibrous mesh. The diameter of the electrospun mesh is about 9 cm and the sealing film has a slightly larger size that is 12×9 cm. After the electrospinning process, the sticky side of the sealing film was carefully placed from one edge gradually to the other edge to cover the entire electrospun fibrous mesh. Thus the entire mesh adhered evenly onto the film. Later the whole electrospun fibrous mesh was easily peeled off from the aluminium foil without any residuals and cut into small slices for humidity detection. This even transferring process guarantees that the variation of thickness between different small slices is minimum. This composite material was used throughout all the experiments. For convenience, we will refer to these composite materials as electrospun fiber mesh from this point, unless specifically indicated.

The whole electrospun fibrous mesh was cut into about 1×1 cm squares or 1×6 cm strips. As shown in the image in Fig. 2b, our material is flexible and has good mechanical strength which will be beneficial for handling and easy to use in further applications. When a piece of this fibrous mesh was covered on top of a well that contained water in a 96 well plate, a round

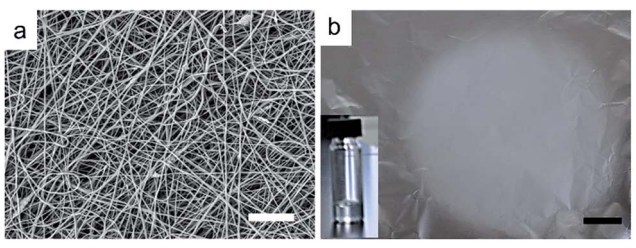

Fig. 1 (a) Morphology of electrospun fibers from 4% w/v PEO polymer solution under a scanning electron microscope. The scale bar is 25 microns. (b) Image of the 4% w/v electrospun fibrous mesh on aluminium foil with a scale bar of 2 cm. The inset image is approximately 1 mL of PEO solution in a 4 mL glass vial.

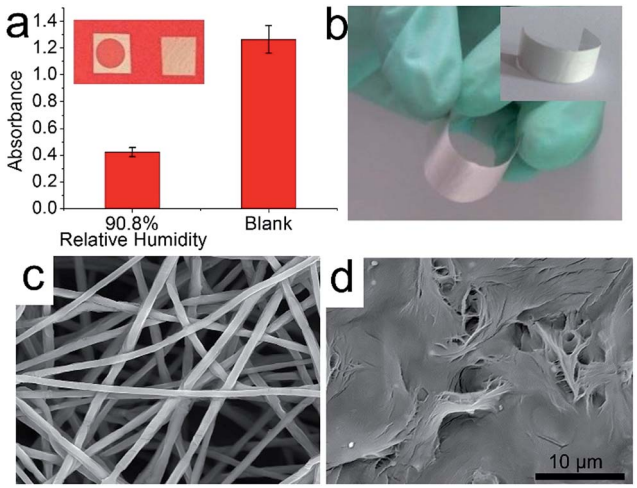

Fig. 2 (a) Image (inset image) and absorbance of the electrospun fibrous mesh before and after exposure to 90.8% relative humidity. Error bar represents the standard deviation ($n = 3$). (b) Flexibility of the electrospun fibrous mesh on an optical clear single-side adhesive film. (c and d) SEM images of electrospun fibers before and after exposure to 90.8% relative humidity, respectively. SEM images (c) and (d) have the same magnification and the scale bar is 10 microns.

shaped transparent spot formed on the fibrous mesh as shown in the inset photo in Fig. 2a. When that photo was taken, a red color paper was placed underneath the fibrous mesh to enhance the contrast. And the absorbance of the fibrous mesh at 400 nm decreased accordingly as shown in Fig. 2a. The SEM image shows a very clear view of what happened. Before exposure to water vapors, fibers can be clearly seen in Fig. 2c. After exposure we can see in Fig. 2d that almost all of the fiber structure

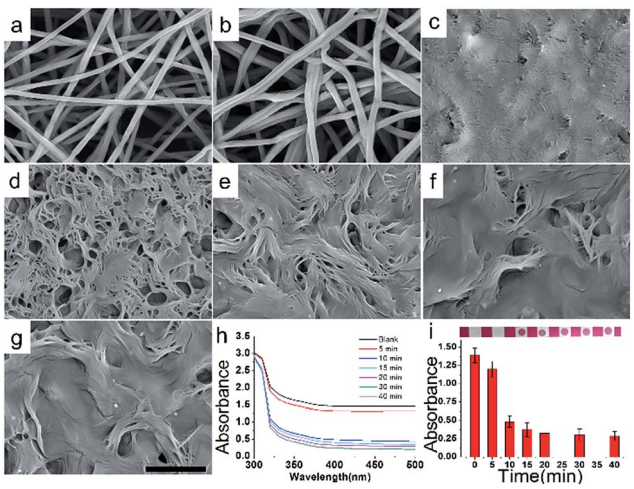

Fig. 3 SEM images of the electrospun fibrous mesh before and after exposure to 90.8% relative humidity for a series of times (a, 0; b, 5; c, 10; d, 15; e, 20; f, 30; g, 40 min). All images have the same magnification and the scale bar is 10 microns; UV-Vis spectra (h) and absorbance (i) of the electrospun fibrous mesh before and after exposure to 90.8% relative humidity for a series of times. Error bar represents the standard deviation ($n = 3$). The inset image in (i) represents the photo of the fibrous mesh.

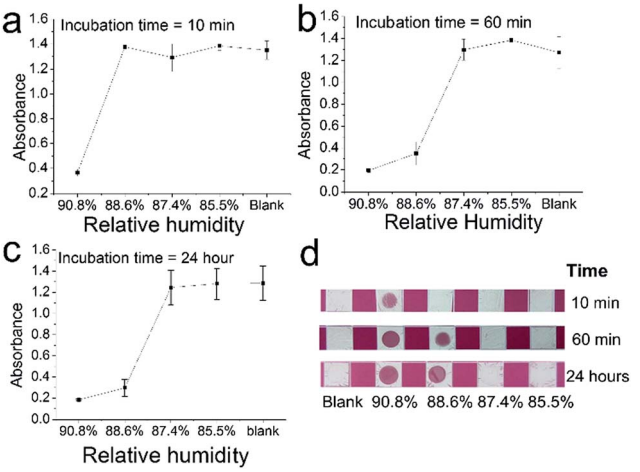

Fig. 4 (a–c) Absorbance of the electrospun fibrous mesh exposed to different relative humidity conditions for 10 min, 60 min, and 24 hours. (d) Images of the electrospun fibrous mesh exposed to different relative humidity conditions for different times. Error bar represents the standard deviation ($n = 3$).

disappeared, however traces of previous fibers are still clear. Thus from the morphology of the remaining structure, we presume that it is caused by the fusion of the fibers. To confirm our assumption, we examined the morphology of the fibrous mesh after different exposure times under SEM.

As shown in Fig. 3a–g, compared with unexposed fibers, after 5 min in 90.8% relative humidity, fibers appear to be slightly curvier than before. Some adjacent fibers start to show signs of merging. After 10 min of exposure, we can clearly see that the fibers melted and fused together to form a film-like structure. After 15 min of exposure, most of the fibers have melted together and only traces of fibers can be seen in the image. The holes are apparently from the empty space between the fibers. From 20 to 40 min of exposure, the surface becomes more and more flat and uniform. From Fig. 3h, we can observe that the absorbance of the electrospun fiber mesh decreases as time increases. From the inset image in Fig. 3i, we can clearly see that a transparent circle formed after 10 min of exposure. For a longer time, the transparency of the fibrous mesh is similar. Since the absorbance is caused by the reflection of the random oriented fibrous fibers, it is almost irrelevant to the wavelength. Thus we can observe very similar absorbance from 400 nm to 600 nm for each kind of fiber in Fig. 3h. Namely, any absorbance of each sample from 400 nm to 600 nm could be chosen to represent its transparency. To test the reproducibility of this phenomenon, we measured the absorbance of all fibrous meshes at 400 nm in triplicate; data are shown in Fig. 3i. For 5 min exposure time, we can observe a slight decrease in absorbance. For 10 min of exposure, the decrease in absorbance is significant. For a longer exposure time, the absorbance decreases slightly until it reaches a plateau after 20 min.

Based on the results we obtained, we utilized this rapid and stable optical transition of the PEO fibrous mesh to sense high humidity. As shown in Fig. 4, if we control the exposure time to be less than 10 min, only 90.8% relative humidity can cause transition of PEO from opaque to transparent. If we extend the exposure time to 60 min, transition starts to occur under 88.6% relative humidity. Surprisingly even when we extended the exposure time to 24 hours, only when the relative humidity was higher than 88.6%, could it induce the transition of the fibrous mesh. This unique phenomenon would make this pure PEO electrospun fibrous mesh a non-toxic, low cost, and practical "cut-off" sensor for high humidity monitoring in food.

We have summarized typical humidity techniques with the best RH range reported so far in Table 1, as well as their response elements. Since our sensor is only composed of a nontoxic polymer, polyethylene oxide, it has the simplest composition (low cost) and minimum possibility for toxicity among these methods, which are critical for food quality monitoring in each individual package. Although the relative humidity range of our methods is narrow, it is quite suitable in the range of moulds and yeasts that infest cereals and rice.

Conclusions

We studied the transition of an electrospun micro/nanofibrous mesh from opaque to transparent by UV-Vis spectroscopy and scanning electron microscopy. We used a water soluble and nontoxic polymer polyethylene oxide (PEO) to fabricate electrospun fibers. In the vapor of water, PEO electrospun fibers start to fuse together, which cause a dramatic decrease at air/fiber interfaces. Due to the random orientation of fibers, light

Table 1 Summary of humidity detection techniques

Techniques	Response elements	RH range[a]	Ref.
Amperometry	Polytetrafluoroethylene film	20–100%	2*a*
Capacitance measurement	Silver nanoparticle	35–90%	2*b*
Resistance measurement	PEDOT:PSS/iron oxide nanoparticle	20–95%	2*c*
Voltage measurement	CuTCNQ/ZnO nanotube arrays	5–90%	2*d*
Quartz crystal microbalance	Polyethyleneimine modified polyamide 6 nano-fiber/net	2–95%	10*b*
Fluorometry	Dapoxyl sulfonic acid	3–96%	3*a*
Colorimetry	Fe_3O_4 nanoparticles	11–97%	7*a*
	$CoCl_2$	5–60%	
Current method	Polyethylene oxide fibrous mesh	88–90%	

[a] RH, relative humidity.

scattering at the air/fiber interface blocked light. As the air/fiber interfaces disappear, the fibrous mesh becomes more and more transparent. At room temperature, the PEO electrospun fibrous mesh becomes transparent in 10 min under 90.8% relative humidity conditions, and takes 60 min for a similar transition in 88.7% relative humidity. Astonishingly, even when we extended the exposure time to 24 hours, the fibrous mesh remained opaque under a slightly lower relative humidity of 87.4%. Thus pure PEO electrospun fibers can be used as a safe, irreversible, equipment-free, and cheap (<\$0.002 per 1×1 cm^2) "cut-off" sensor for high humidity monitoring when low toxicity and irreversibility are highly required, such as in rice and cereals.

Acknowledgements

We thank the National Natural Science Foundation of China (Grant no. 21305083), Changjiang Scholars and Innovative Research Team in University (Grant no. IRT 1124), and Fundamental Research Funds for the Central Universities (Grant no. GK201303003 and GK201402051) for financial support.

Notes and references

1 H. W. Yu, H. K. Kim, T. Kim, K. M. Bae, S. M. Seo, J. M. Kim, T. J. Kang and Y. H. Kim, *ACS Appl. Mater. Interfaces*, 2014, **6**, 8320.

2 (*a*) H. Guo, J. Chen, L. Tian, Q. Leng, Y. Xi and C. Hu, *ACS Appl. Mater. Interfaces*, 2014, **6**, 17184; (*b*) M. Mraović, T. Muck, M. Pivar, J. Trontelj and A. Pleteršek, *Sensors*, 2014, **14**, 13628–13643; (*c*) S. Taccola, F. Greco, A. Zucca, C. Innocenti, C. d. J. Fernández, G. Campo, C. Sangregorio, B. Mazzolai and V. Mattoli, *ACS Appl. Mater. Interfaces*, 2013, **5**, 6324; (*d*) K. Wang, X. Qian, L. Zhang, Y. Li and H. Liu, *ACS Appl. Mater. Interfaces*, 2013, **5**, 5825–5831; (*e*) P. Su and C. Wang, *Sens. Actuators, B*, 2007, **123**, 1071; (*f*) S. Hwang, D. Kang, R. S. Ruoff, H. S. Shin and Y. B. Park, *ACS Nano*, 2014, **8**, 6739; (*g*) T. Munoz Jr and K. J. Balkus Jr, *Chem. Mater.*, 1998, **10**, 4114; (*h*) R. Demir, S. Okur and M. Şeker, *Ind. Eng. Chem. Res.*, 2012, **51**, 3309.

3 (*a*) J. C. Tellis, C. A. Strulson, M. M. Myers and K. A. Kneas, *Anal. Chem.*, 2011, **83**, 928; (*b*) E. Kim, S. Yeon Kim, G. Jo, S. Kim and M. J. Park, *ACS Appl. Mater. Interfaces*, 2012, **4**, 5179; (*c*) D. Bridgeman, J. Corral, A. Quach, X. Xian and E. Forzani, *Langmuir*, 2014, **30**, 10785; (*d*) K. Sulvegh and R. Zelko, *Macromolecules*, 2002, **35**, 795.

4 (*a*) M. Beyer, J.-A. Verreet and W. Ragab, *Int. J. Food Microbiol.*, 2005, **98**, 233–240; (*b*) S. Choi, H. Jun, J. Bang, S.-H. Chung, Y. Kim, B. Kim, H. Kim, L. Beuchat and J.-H. Ryu, *Food Microbiol.*, 2015, **46**, 307–313; (*c*) J. Gilbert, S. M. Woods and U. Kromer, *Phytopathology*, 2008, **98**, 504.

5 S. Choi, H. Kim, Y. Kim, B. Kim, L. Beuchat and J.-H. Ryu, *Food Microbiol.*, 2014, **38**, 122–127.

6 (*a*) A. Léonard and R. Lauwerys, *Mutat. Res., Rev. Genet. Toxicol.*, 1990, **239**, 17–27; (*b*) L. S. Nelson, N. A. Lewin, M. A. Howland, R. S. Hoffman, L. R. Goldfrank and N. E. Flomenbaum, *Goldfrank's Toxicologic Emergencies*, New York, McGraw Hill, 9th edn, 2011; (*c*) S. J. Stohs and D. Bagchi, *Free Radical Biol. Med.*, 1995, **18**, 321.

7 (*a*) H. Hu, Q. Chen, K. Cheng and J. Tang, *J. Mater. Chem.*, 2012, **22**, 1021; (*b*) H. Wang and K. Zhang, *Sensors*, 2013, **13**, 4192; (*c*) N. A. Luechinger, S. Loher, E. K. Athanassiou, R. N. Grass and W. J. Stark, *Langmuir*, 2007, **23**, 3473.

8 (*a*) N. Bhardwaj and S. C. Kundu, *Biotechnol. Adv.*, 2010, **28**, 325; (*b*) D. Li and Y. N. Xia, *Adv. Mater.*, 2004, **16**, 1151; (*c*) A. Greiner and J. H. Wendorff, *Angew. Chem., Int. Ed.*, 2007, **46**, 5670.

9 C. Zhou, Y. Shi, X. Ding, M. Li, J. Luo, Z. Lu and D. Xiao, *Anal. Chem.*, 2013, **85**, 1171.

10 (*a*) W. Zheng, X. Lu, W. Wang, Z. Li, H. Zhang, Z. Wang, X. Xu, S. Li and C. Wang, *J. Colloid Interface Sci.*, 2009, **338**, 366; (*b*) X. Wang, B. Ding, J. Yu and M. Wang, *J. Mater. Chem.*, 2011, **21**, 16231.

11 V. O. Sheftel, *Indirect Food Additives and Polymers: Migration and Toxicology*, CRC Press, 2000.